Research Article | Vol. 25, No. 10 | 15 May 2017 | OPTICS EXPRESS 10893

Optics EXPRESS

Ultra-compact MMI-based beam splitter demultiplexer for the NIR/MIR wavelengths of 1.55 μm and 2 μm

M-SAID ROUIFED,[1,*] CALLUM G. LITTLEJOHNS,[1,2] GUO X. TINA,[1] HAODONG QIU,[1] JORDI SOLER PENADES,[2] MILOS NEDELJKOVIC,[2] ZECEN ZHANG,[1] CHONGYONG LIU,[1] DAVID J. THOMSON,[2] GORAN Z. MASHANOVICH,[2] GRAHAM T. REED,[2] AND HONG WANG[1]

[1]*Silicon Technologies Centre of Excellence, Department of electronic and electrical engineering, Nanyang Technological University, Singapore 639798, Singapore*
[2]*Optoelectronics Research Centre, University of Southampton, Southampton, SO17 1BJ, UK*
[*]*m-said.rouifed@ntu.edu.sg*

Abstract: Based on restricted interferences mechanism in a 1x2 MMI beam splitter, we theoretically investigate and experimentally demonstrate an ultra-compact MMI-based demultiplexer for the NIR/MIR wavelengths of 1.55 μm and 2 μm. The device is fabricated on 340 nm SOI platform, with a footprint of 293x6 μm^2. It exhibits extremely low insertion losses of 0.14 dB and 1.2 dB at the wavelengths of 1.55 μm and 2 μm, respectively, with contrasts of approximately 20 dB for both wavelengths, and a cross-talk of 18.83 dB.

OCIS codes: (230.0230) Optical devices; (230.1360) Beam splitters.

References and links

1. D. J. Thomson, C. G. Littlejohns, S. Stanković, and S. A. R. M. Nedeljkovic, *Silicon Photonics* (Wiley Encyclopedia of Electrical and Electronics Engineering, 2015), pp. 1–22.
2. N. K. Hon, R. Soref, and B. Jalali, "The third-order nonlinear optical coefficients of Si, Ge, and $Si_{1-x}Ge_x$ in the midwave and longwave infrared," J. Appl. Phys. **110**(1), 011301 (2011).
3. F. De Leonardis, B. Troia, R. A. Soref, and V. M. N. Passaro, "Investigation of germanium Raman lasers for the mid-infrared," Opt. Express **23**(13), 17237–17254 (2015).
4. M. Nedeljkovic, R. A. Soref, and G. Z. Mashanovich, "Free-carrier electro-absorption and electro-refraction modulation in group IV materials at mid-infrared wavelengths," Proc. SPIE **8266**, 82660Y (2012).
5. Y. Chen, H. Lin, J. Hu, and M. Li, "Heterogeneously integrated silicon photonics for the mid-infrared and spectroscopic sensing," ACS Nano **8**(7), 6955–6961 (2014).
6. G. Z. Mashanovich, F. Y. Gardes, D. J. Thomson, Y. Hu, K. Li, M. Nedeljkovic, J. S. Penadés, A. Z. Khokhar, C. J. Mitchell, S. Stankovic, R. Topley, S. A. Reynolds, Y. Wang, B. Troia, V. M. N. Passaro, C. G. Littlejohns, T. D. Bucio, P. R. Wilson, and G. T. Reed, "Silicon photonic waveguides and devices for near- and mid-IR applications," IEEE J. Sel. Top. Quantum Electron. **21**(4), 8200112 (2015).
7. R. Soref, "Mid-infrared photonics in silicon and germanium," Nat. Photonics **4**(8), 495–497 (2010).
8. M. Nedeljkovic, J. S. Penadés, A. Z. Khokhar, C. J. Mitchell, S. Stankovic, T. B. Dominguez, C. G. Littlejohns, F. Y. Gardes, and G. Z. Mashanovich, "Grating coupled low loss Ge-on-Si waveguides and multimode interferometers for the mid-infrared," in Optical Fibre Communication Conference, OSA Technical Digest Series (Optical Society of America, 2015), paper WA4.3.
9. P. Biagioni, J. Frigerio, A. Samarelli, K. Gallacher, L. Baldassarre, E. Sakat, E. Calandrini, R. W. Millar, V. Giliberti, G. Isella, D. J. Paul, and M. Ortolani, "Group-IV midinfrared plasmonics," J. Nanophotonics **9**(1), 093789 (2015).
10. M.-S. Rouifed, C. G. Littlejohns, G. X. Tina, Q. Haodong, T. Hu, Z. Zhang, C. Liu, G. T. Reed, and H. Wang, "Low loss SOI waveguides and MMIs at the MIR wavelength of 2 μm," IEEE Photonics Technol. Lett. **28**(24), 2827–2829 (2016).
11. A. Malik, M. Muneeb, Y. Shimura, J. V. Campenhout, R. Loo, and G. Roelkens, "Germanium-on-silicon planar concave grating wavelength (de)multiplexers in the mid-infrared," Appl. Phys. Lett. **103**(16), 161119 (2013).
12. Y. Hu, R. M. Jenkins, F. Y. Gardes, E. D. Finlayson, G. Z. Mashanovich, and G. T. Reed, "Wavelength division (de)multiplexing based on dispersive self-imaging," Opt. Lett. **36**(23), 4488–4490 (2011).
13. Z. Li, A. M. Heidt, N. Simakov, Y. Jung, J. M. O. Daniel, S. U. Alam, and D. J. Richardson, "Diode-pumped wideband thulium-doped fiber amplifiers for optical communications in the 1800 - 2050 nm window," Opt. Express **21**(22), 26450–26455 (2013).

#290380 https://doi.org/10.1364/OE.25.010893
Journal © 2017 Received 9 Mar 2017; revised 18 Apr 2017; accepted 18 Apr 2017; published 2 May 2017

Optics EXPRESS

14. F. Poletti, N. V. Wheeler, M. N. Petrovich, N. Baddela, E. Numkam, J. R. Hayes, D. R. Gray, Z. Li, R. Slavík, and D. J. Richardson, "Towards high-capacity fibre-optic communications at the speed of light in vacuum," Nat. Photonics **7**(4), 279–284 (2013).
15. J. J. Ackert, D. J. Thomson, L. Shen, A. C. Peacock, P. E. Jessop, G. T. Reed, G. Z. Mashanovich, and A. P. Knights, "High-speed detection at two micrometres with monolithic silicon photodiodes," Nat. Photonics **9**(6), 393–396 (2015).
16. B. Souhan, R. R. Grote, C. P. Chen, H.-C. Huang, J. B. Driscoll, M. Lu, A. Stein, H. Bakhru, K. Bergman, W. M. J. Green, and R. M. Osgood, "Si+-implanted Si-wire waveguide photodetectors for the mid-infrared," Opt. Express **22**(22), 27415–27424 (2014).
17. M. N. Petrovich, F. Poletti, J. P. Wooler, A. M. Heidt, N. K. Baddela, Z. Li, D. R. Gray, R. Slavík, F. Parmigiani, N. V. Wheeler, J. R. Hayes, E. Numkam, L. Grűner-Nielsen, B. Pálsdóttir, R. Phelan, B. Kelly, J. O'Carroll, M. Becker, N. MacSuibhne, J. Zhao, F. C. G. Gunning, A. D. Ellis, P. Petropoulos, S. U. Alam, and D. J. Richardson, "Demonstration of amplified data transmission at 2 μm in a low-loss wide bandwidth hollow core photonic bandgap fiber," Opt. Express **21**(23), 28559–28569 (2013).
18. K.-C. Lin and W.-Y. Lee, "Guided-wave 1.3/1.55 μm wavelength division multiplexer based on multimode interference," Electron. Lett. **32**(14), 1259–1261 (1996).
19. J. Xiao, X. Liu, and X. Sun, "Design of an ultracompact MMI wavelength demultiplexer in slot waveguide structures," Opt. Express **15**(13), 8300–8308 (2007).
20. B. B. B. Zaken, T. Zanzury, and D. Malka, "An 8-Channel Wavelength MMI demultiplexer in slot waveguide structure," Mater. Lett. **9**(881), 1–10 (2016).
21. S.-L. Tsao, H.-C. Guo, and C.-W. Tsai, "A novel 1 × 2 single-mode 1300/1550 nm wavelength division multiplexer with output facet-tilted MMI waveguide," Opt. Commun. **232**(1–6), 371–379 (2004).
22. A. Y. Piggott, J. Lu, K. G. Lagoudakis, J. Petykiewicz, T. M. Babinec, and J. Vučković, "Inverse design and demonstration of a compact and broadband on-chip wavelength demultiplexer," Nat. Photonics **9**(6), 374–377 (2015).
23. H. Lin, Z. Yi, and J. Hu, "Double resonance 1-D photonic crystal cavities for single-molecule mid-infrared photothermal spectroscopy: theory and design," Opt. Lett. **37**(8), 1304–1306 (2012).
24. L. B. Soldano and E. C. M. Pennings, "Optical multi-mode interference devices based on self-imaging: principles and applications," J. Lightwave Technol. **13**(4), 615–627 (1995).
25. Online Available: https://www.lumerical.com/tcad-products/mode/EME.

1. Introduction

Silicon photonics for near infrared (NIR) applications dates back to the 1980s [1]. In the last decade, intensive research has been conducted on the emerging silicon photonics for mid-infrared (MIR) domain (2-20 μm) [2–9]. Long-wavelength optoelectronic devices on silicon are important for low cost and high levels of integration. Many sensing and detection applications will benefit from the compact devices, low cost and commercial scalability that will be enabled by a silicon photonics platform [7].

In order to achieve full integration of the main building blocks of communication systems and lab-on-a-chip devices, passive components are of paramount importance. Therefore, they should be designed and developed. In the MIR spectral range from 2 μm to 5 μm, several devices have been proposed to perform different optical functionalities, such as Mach-Zehnder interferometers [6], multimode interference (MMI) couplers [10], arrayed waveguide de-multiplexers [11], and angled MMI-based de-multiplexers [12]. Such devices have been developed using different platforms, depending on the targeted operating MIR wavelengths.

A particular interest is devoted to the wavelength of 2 μm to exploit the amplification capabilities of the direct diode-pumped monolithic thulium-doped fiber amplifier (TDFA) [13], the low-loss and low latency potential of transmission systems based on hollow core photonic band gap fibers (HC-PBGF) [14], and the high speed capabilities of silicon-based photodetectors [15,16]. HC-PBGFs, with a minimum loss observed around 2 μm, offer a radical solution to increase transmission capacity per fiber, decrease fiber loss and nonlinearity, and reduce signal latency when compared to the state-of-the-art in the traditional [17] communication bands of 1.3 μm and 1.55 μm.

Wavelength division multiplexer (WDM) play a key role for demultiplexing 1.3 μm and 1.55 μm in optical telecommunication systems. Several works have been performed to design an MMI-based demultiplexer in order to split the two telecommunication wavelengths, using the restricted interference mechanism [18–21], or an inverse design algorithm [22]. To the best of our knowledge, there has not been any demonstration of such components for

Optics EXPRESS

NIR/MIR wavelengths. Nevertheless this component could be an essential element in future optical telecommunication systems, such as fiber to the home (FTTH) system. Moreover, the emerging absorption spectrometers based on MIR pump / NIR probe configuration will need high efficient WDMs for NIR/MIR wavelengths [23].

In this work, we present a new design for a compact guided-wave 1.55/2 μm wavelength division multiplexer based on multimode interference (MMI), using the restricted interference mechanism. Our choice of this structure and concept are based on their characteristics; including the compactness, wide optical bandwidth and high fabrication tolerances. The device has been simulated to optimize its dimensions, and subsequently fabricated using a 340 nm silicon-on-insulator (SOI) platform [10]. Finally, measurements have been performed to evaluate its optical performances. This device exhibits high capability of demultiplexing the NIR and MIR wavelengths of 1.55 μm and 2 μm with an extremely low insertion loss (approximately 1 dB) and high contrast (approximately 20 dB), with a footprint of 293x6 μm^2. Furthermore, we demonstrate that such a component is able to work either as a demultiplexer or a multiplexer, depending on the optical mode input.

2. Operating principles and simulation

The operating principle of the MMI structure is based on the self-image effect [24]. This mechanism involves the excitation of multiple guided-modes in the multimode waveguide region in order to interfere constructively and produce a single image, or multiple images, of the launched optical mode. These images appear at periodic intervals along the propagation direction. However, if restrictions are placed on the modal excitations (the so-called "restricted interferences regime"), only certain modes in the multimode waveguide region will be excited. This leads to the occurrence of a direct or mirrored image of the launched optical mode. In order to achieve the restricted interference mechanism, the input/output of a 1x2 MMI coupler should be positioned at ± $W_{MMI}/6$ with respect to the center of the MMI region (W_{MMI}: MMI width). At this position, every third mode will not be excited, and the optical output image will appear at:

$$L_{MMI} = pL_{\pi} \tag{1}$$

where L_{MMI} is the MMI length, p is an integer, and L_{π} is the beat length defined as:

$$L_{\pi} = \frac{4n_{eff}W_e^2}{3\lambda_0} \tag{2}$$

where λ_0 is the wavelength, n_{eff} is the effective refractive index, and W_e ($\approx W_{MMI}$) is the effective width, which can be approximated to the width of the MMI structure [24]

Based on this mechanism, we propose a wavelength demultiplexer device using an MMI structure for the 1.55 μm and 2 μm wavelengths. The schematic view of the device is depicted in Fig. 1. It consists of three parts: part one is the input waveguide (port 1), which is tapered from a single mode waveguide (@ 1.55 μm and 2 μm) to 1.3 μm and shifted from the MMI's center by 1.5 μm. Part two is the multimode region. In order to reduce the beat length of the MMI and avoid optical coupling between the two output-waveguides, we fixed the width to 6 μm. Part 3 is the output waveguides (ports 2 & 3), shifted from the center of the MMI by 1.5 μm, and tapered down from 1.3 μm to single-mode waveguide width.

The operating principle of this device is: when two wavelengths of 1.55 μm and 2 μm are launched in the input waveguide (port 1), they can be separated into port 2 and port 3 by forming a direct image for 2 μm wavelength at port 3, and a mirrored image for 1.55 μm at port 2. To achieve this behavior, the length of the MMI should satisfy Eq. (1) for both wavelengths, which leads to the following condition:

$$L_{MMI} = pL_{\pi}^{\lambda_1} = (p+q)L_{\pi}^{\lambda_2} \tag{3}$$

Optics EXPRESS

where p is an integer, q is an odd integer, and $L_\pi^{\lambda_i}$ is the beat length at the wavelength λ_i.

To determine the length of the MMI for which the separation of the two wavelengths is achieved, we performed some simulations using the Eigen-Mode Expansion (EME) solver from Lumerical [25]. Table 1 details the MMI parameters and their optimized dimensions. In the simulations, an optical mode (TE) is launched at port (1) and the transmitted power at the output ports is recorded as a function of the MMI's length. Figure 2 shows the results for both 1.55 μm and 2 μm. At 1.55 μm, it can be seen that the maximum and minimum transmission is achieved for an MMI length of 290-300 μm at port 2 and port 3, respectively (Fig. 2(a)). For the same length (around 290-300 μm), the max/min transmission is obtained at ports 3/2 respectively for the wavelength of 2 μm (Fig. 2(b)). As a result, a direct image of the launched mode is formed for the wavelength of 2 μm at port 3, which corresponds to the bar-state, and a mirrored image is formed at port 2 for the wavelength of 1.55 μm, which corresponds to the cross-state.

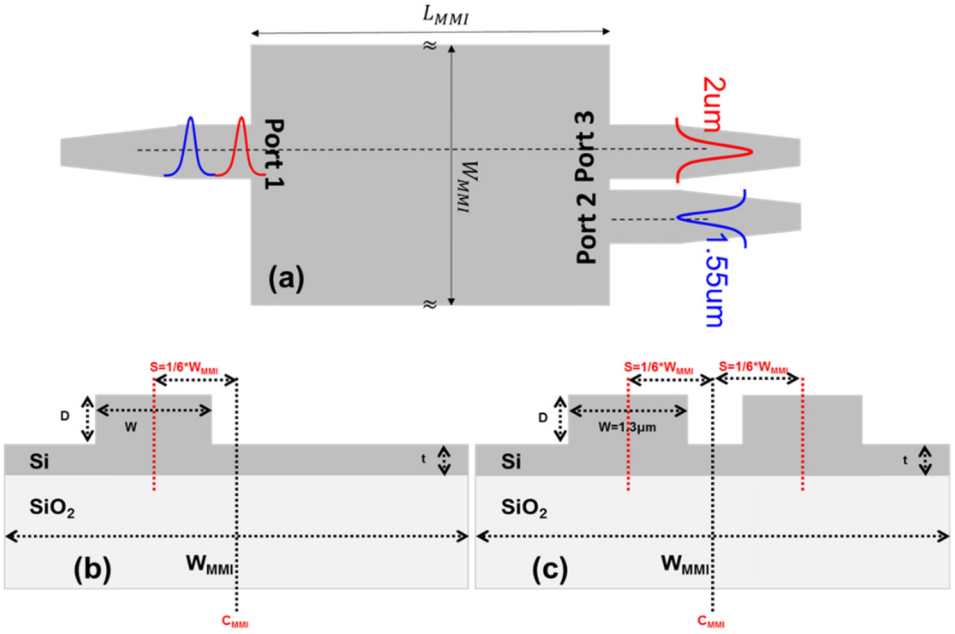

Fig. 1. Schematic view of the MMI-DeX (a) top view, (b) input cross-section view, (c) output cross-section view.

We should highlight that this length is not the only length that satisfies Eq. (3); however, it is the shortest. At each operating wavelength, the performance of this device can be evaluated in terms of insertion loss (IL) and contrast (C) by the following:

$$IL = -10Log_{10}\left(\frac{P_i}{P_1}\right) \tag{4}$$

$$C = 10Log_{10}\left(\frac{P_i}{P_j}\right) \tag{5}$$

where $P_i \neq P_j$ is the power at ports 2 and 3, and P_1 is the power at port 1 (input power). Figure 3(a) and 3(b) show the simulated contrast and insertion loss as a function of MMI length in the range 282-294 μm. It can be seen that the contrast achieved is higher than 20 dB, and insertion losses are less than 1 dB for a wide range of lengths. The power intensity profiles

Optics EXPRESS

are reported in Fig. 3(c) and 3(d). It is clearly observed that the optical power is transmitted through port 2 for a wavelength of 1.55 μm, and port 3 for a wavelength of 2 μm, with an MMI length of 290 μm.

Table 1. Dimensions of the simulated MMI device

Parameters	W_{MMI}	S	$W_{in} = W_{out}$	D	t
Dimensions [μm]	6	1.5	1.3	0.24	0.1

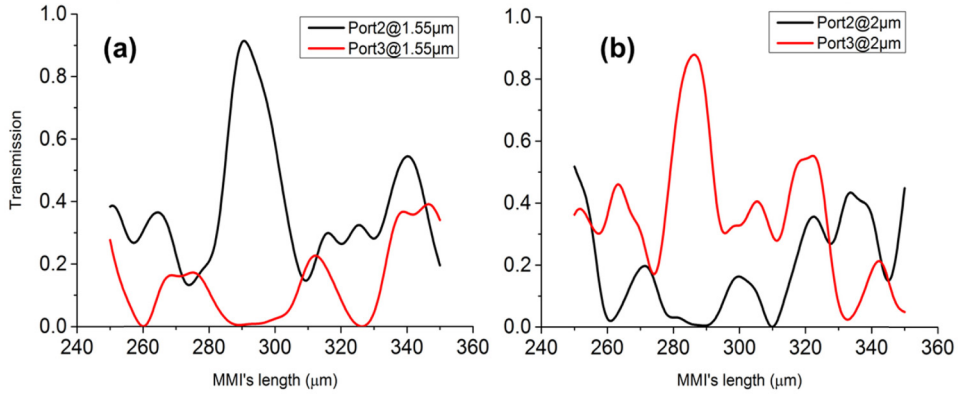

Fig. 2. Transmission at the two output ports for: (a) 1.55 μm and (b) 2 μm.

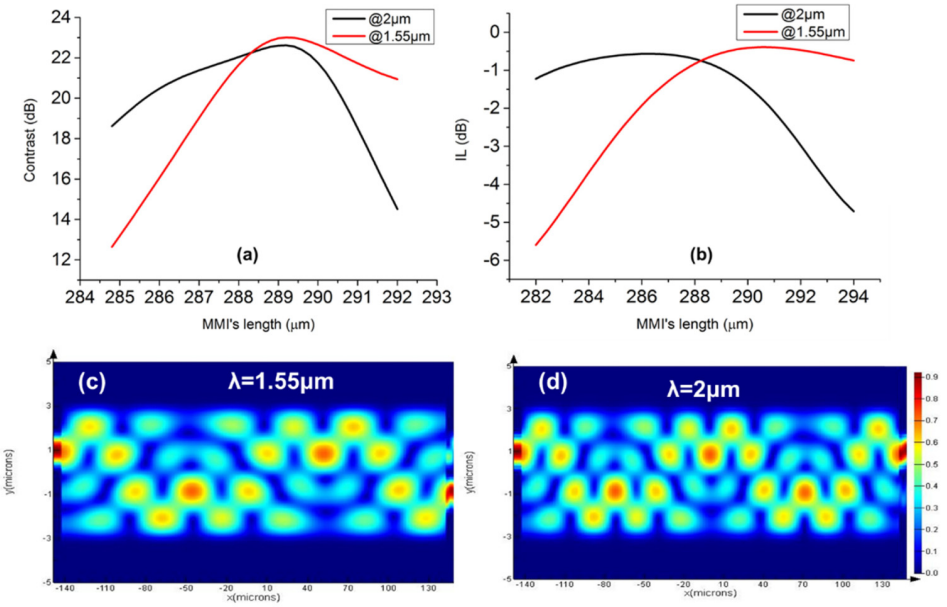

Fig. 3. MMI-DeX simulated performance (a) The contrast and (b) the insertion loss of the MMI-based DeX as a function of the MMI's length for the wavelengths of 1.55 μm and 2 μm. Simulated power intensity profile at (c) 1.55 μm and (d) 2 μm wavelength for an MMI length of 290 μm.

3. Fabrication and characterization results

The fabrication of the MMI-based demultiplexer was carried out using an SOI substrate with a 2 μm-thick buried oxide (BOX), and 340 nm-thick silicon overlayer. Two fabrication steps

Optics EXPRESS

were used to define the surface grating couplers and rib-waveguides with etch depths of 140 nm and 240 nm respectively. Separate grating couplers were designed to work at each wavelength (1.55 μm & 2 μm), with the same etch depth but different pitch. The use of grating coupling instead of butt coupling necessitated the need to replicate each device with a different input/output grating coupler at ports 1/2/3, in order to be able to characterize the device at both wavelengths. All lithography steps were carried out using ZEP A520 resist and a Vistec EBPG5200 e-beam lithography system. Silicon etching was performed using a mixture of SF_6 and C_4F_8 gases in a deep reactive ion etching (DRIE) system. Following this etch, an oxide cladding layer of 200 nm was deposited using PECVD system. Figure 4(a) shows a scanning electron microscope (SEM) image of the input/output grating couplers, and Fig. 4(b) shows an SEM image of the MMI's output. According to the simulations, the optimal length of the MMI is around 290 μm; hence, we included length variations in our design (from 285 μm to 293 μm) in order to study the changes in the optical output as a function of the MMI's length.

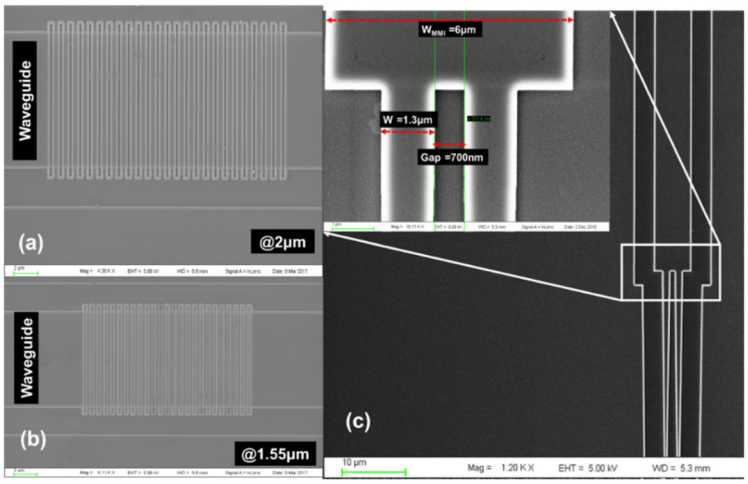

Fig. 4. SEM image of the input/output grating coupler, (a) @ 2 μm and (b) @ 1.55 μm, (c) SEM image of the two output waveguides of the MMI. The width of the MMI and waveguides are 6 μm and 1.3 μm respectively. The gap between the two waveguides is 700 nm.

The devices were characterized using a "Thorlabs" pigtailed FP laser diode for 2 μm wavelength, and a TunicsT100SHP laser for 1.55 μm wavelength. A linearly TE-polarized light beam from the polarization controller was coupled to the MMI's input through the surface grating coupler. After propagation through the device, the output power was coupled back into a fiber and sent to an extended InGaAs photodetector (it is able to measure both wavelengths).

The transmitted power was recorded as a function of the MMI length for both wavelengths (1.55 μm & 2 μm) and both output ports (port 2 & port 3). The recorded data was normalized to transmission waveguides of the same length as the MMI, but without the interference region. This normalization method is very useful to separate the device loss from the coupling loss due to the grating couplers, and other system losses such as fiber loss. In Fig. 5(a), the transmission of the MMI as a function of MMI length is reported for both output ports at a wavelength of 2 μm. As predicted in our simulations, the power measured is higher in port 3 than port 2 because it corresponds to the bar-state (direct image of the launched field) for this wavelength. The insertion loss is less than 5 dB for all the fabricated MMI lengths, with an optimal length of 289 μm (insertion loss = 0.8 dB). At this length, the contrast is calculated to be 20.46 dB (blue dashed line in Fig. 5(a)). The same behavior is observed in Fig. 5(b), where the output power is recorded at the wavelength of 1.55 μm. In

Optics EXPRESS

this case, the maximum transmission is observed at port 2, and the minimum transmission at port 3. Clearly, this configuration corresponds to the cross-state (mirrored image of the launched field) at 1.55 μm. At this wavelength, the lowest insertion loss of 0.14 dB is measured for a length of 293 μm, with a contrast of 19.83 dB.

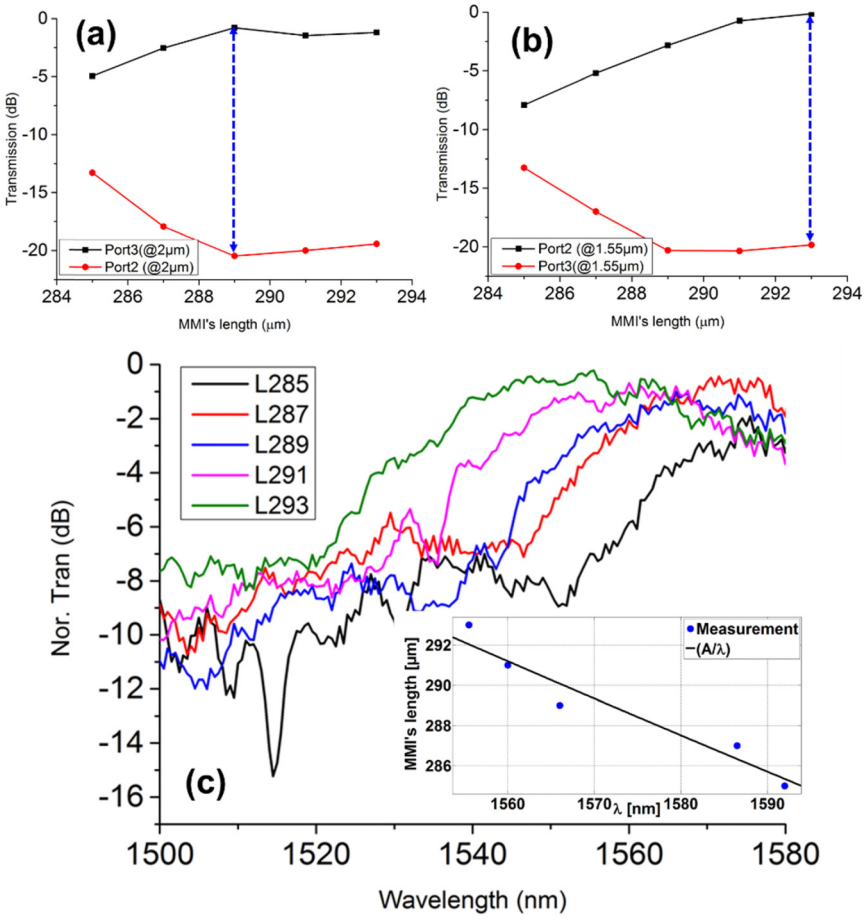

Fig. 5. (a) & (b) The transmission through the two output waveguides at 2 μm and 1.55 μm as a function of MMI length. Dashed blue arrows show where the maximum contrast is obtained. (c) Transmission spectra of the MMI at NIR wavelengths for different lengths measured at port 3. Inset: Optimal MMI length (in terms of insertion loss) as a function of the wavelength.

From these results, it is clear that the optimal length is not the same for both wavelengths. However, a trade-off between the IL/Contrast and the MMI length results in an optimal length of 293 μm. Here, the insertion losses are 0.14 dB and 1.2 dB at 1.55 μm and 2 μm, respectively, and the contrast is 19.83 dB and 19.42 dB at 1.55 μm and 2 μm, respectively. The cross-talk between the two wavelengths at this MMI length is 18.83 dB.

The normalized transmission spectra of different MMI lengths at 1.55 μm are shown in Fig. 5(c). As it can be observed, there is a blue-shift (shift to the shorter wavelengths) of the transmission when the length of the MMI is increased. According to Eq. (2), the beat length L_π (or L_{MMI}) is inversely proportional to the wavelength, therefore the optimal MMI length for shorter wavelengths is longer than one for longer wavelengths, hence the blue-shift of the spectra. Inset in Fig. 5, we report the length of the MMI as a function of the wavelength where the maximum power is recorded (i.e. the minimum insertion loss). By combining Eq.

Optics EXPRESS

(2) and (3), we have fitted this data, and we can see that our calculation fits reasonably well the experimental data (with 95% of confidence bounds in Matlab).

In order to test the device as a multiplexer, we inverted the positions of the input to output, and by keeping the same coupling conditions we observed that the recorded power remains the same compared to the first configuration. Hence, this leads us to the conclusion that the device can work either as a demultiplexer or a multiplexer, depending on the propagation direction.

4. Conclusion

In summary, an MMI-based beam splitter demultiplexer is theoretically investigated and experimentally demonstrated. Based on restricted interference mechanism, we designed an ultra-compact device where both NIR (1.55 μm) and MIR (2 μm) wavelengths have been successfully separated. The 293 μm long device exhibits insertion losses of 0.14 dB and 1.2 dB at 1.55 μm and 2 μm, respectively, and a contrast of 19.83 dB and 19.42 dB at 1.55 μm and 2 μm, respectively. Furthermore, the cross-talk between the two wavelengths is 18.83 dB. As our proposed MMI-based demultiplexer can offer attractive features such as compactness, large fabrication tolerance, and CMOS compatibility, it can be a promising candidate for future silicon photonic transceivers.

Funding

National Research Foundation of Singapore (NRFCRP12-2013-04) and NTU-A*Star Silicon Technologies Centre of Excellence.